Chemical insights, explicit chemistry, and yields of secondary organic aerosol from OH radical oxidation of methylglyoxal and glyoxal in the aqueous phase

Y. B. Lim[1], Y. Tan[2], and B. J. Turpin[1]

[1]Department of Environmental Sciences, Rutgers University, New Brunswick, NJ, USA
[2]Center for Atmospheric Particle Studies, Carnegie Mellon University, Pittsburgh, PA, USA

Correspondence to: Y. B. Lim (ylim@envsci.rutgers.edu)

Abstract. Atmospherically abundant, volatile water-soluble organic compounds formed through gas-phase chemistry (e.g., glyoxal (C_2), methylglyoxal (C_3), and acetic acid) have great potential to form secondary organic aerosol (SOA) via aqueous chemistry in clouds, fogs, and wet aerosols. This paper (1) provides chemical insights into aqueous-phase OH-radical-initiated reactions leading to SOA formation from methylglyoxal and (2) uses this and a previously published glyoxal mechanism (Lim et al., 2010) to provide SOA yields for use in chemical transport models. Detailed reaction mechanisms including peroxy radical chemistry and a full kinetic model for aqueous photochemistry of acetic acid and methylglyoxal are developed and validated by comparing simulations with the experimental results from previous studies (Tan et al., 2010, 2012). This new methylglyoxal model is then combined with the previous glyoxal model (Lim et al., 2010), and is used to simulate the profiles of products and to estimate SOA yields.

At cloud-relevant concentrations ($\sim 10^{-6} - \sim 10^{-3}$ M; Munger et al., 1995) of glyoxal and methylglyoxal, the major photooxidation products are oxalic acid and pyruvic acid, and simulated SOA yields (by mass) are $\sim 120\%$ for glyoxal and $\sim 80\%$ for methylglyoxal. During droplet evaporation oligomerization of unreacted methylglyoxal/glyoxal that did not undergo aqueous photooxidation could enhance yields. In wet aerosols, where total dissolved organics are present at much higher concentrations (~ 10 M), the major oxidation products are oligomers formed via organic radical–radical reactions, and simulated SOA yields (by mass) are $\sim 90\%$ for both glyoxal and methylglyoxal. Non-radical reactions (e.g., with ammonium) could enhance yields.

1 Introduction

Water is predicted to be the largest component of fine particles ($PM_{2.5}$) globally (Liao and Seinfeld, 2005) and in regions with high relative humidity and hygroscopic aerosol species. Water in clouds, fogs, and aerosols provides an abundant and important medium for chemistry, including chemistry that forms secondary organic aerosol (SOA).

The vast majority of organics are emitted in the gas phase. Gas-phase photochemistry fragments and oxidizes these emissions, making water-soluble organics (e.g., acetic acid, glyoxal) ubiquitous and abundant in the atmosphere (Millet et al., 2005). Recent laboratory, field and modeling studies suggest that several water-soluble organic compounds dissolve in atmospheric waters (e.g., cloud/fog droplets and wet aerosols) and undergo aqueous radical and non-radical chemistry to form SOA (e.g., Blando and Turpin, 2000; Ervens et al., 2011; Gong et al., 2011; Myriokefalitakis et al., 2011; Lee et al., 2011, 2012; Zhou et al., 2011; Tan et al., 2012; Ortiz-Montalvo et al., 2012; J. Liu et al., 2012; Y. Liu et al., 2012; Lin et al., 2012; McNeill et al., 2012). Hereafter, this type of SOA is denoted as aqSOA.

In a previous publication (Lim et al., 2010), we developed a full kinetic model including detailed radical chemistry to describe aqSOA formation via OH radical oxidation of glyoxal, an abundant and highly water-soluble compound

formed through photooxidation of alkenes and aromatics. The current work is focused on methylglyoxal. Methylglyoxal is a common α-carbonyl in the atmosphere (Munger et al., 1995), with a globally estimated source of 140 Tg annually (Fu et al., 2008). It is formed from the photooxidation of both anthropogenic VOCs like aromatic hydrocarbons (Nishino et al., 2010) and biogenic VOCs including isoprene (Atkinson et al., 2006). The major sinks are gas-phase UV photolysis and photooxidation (Tadic et al., 2006; Fu et al., 2008). Like glyoxal, methylglyoxal also has great potential to form SOA through aqueous-phase reactions in clouds and wet aerosols, due to its high water solubility ($H_{eff} = 3.71 \times 10^3$ M atm^{-1}; Betterton and Hoffmann, 1988), ability to form oligomers via acid catalysis, and reactivity with OH radicals (Blando and Turpin, 2000; De Haan et al., 2009; Sareen et al., 2010; Tan et al., 2010, 2012). Acetic acid ($H_{eff} = 5.50 \times 10^3$ M atm^{-1}; Herrmann et al., 2005) is highly water soluble, atmospherically abundant both in the gas phase (~ 300 ppt; Nolte et al., 1999) and in the aqueous phase (Khare et al., 1999), and also a major intermediate product of methylglyoxal + OH (Tan et al., 2012). It should be noted that methylglyoxal and acetic acid are much more reactive with OH radicals in the aqueous phase than in the gas phase (lifetimes in the aqueous phase are ~ 26 min for methylglyoxal and ~ 17 h for acetic acid; however, in the gas phase, lifetimes are ~ 0.9 day for methylglyoxal and 17 days for acetic acid).

In this paper, a full kinetic model for the aqueous OH radical oxidation of methylglyoxal is proposed. Detailed radical chemistry includes peroxy radical (RO$_2$) chemistry initiated by bimolecular reactions (RO$_2$–RO$_2$ reactions). We validate, in part, the methylglyoxal model by comparing results from aqueous photooxidation experiments developed by Tan et al. (2010, 2012) with model simulations of these experiments. Note that in aqueous photooxidation experiments, OH radicals are formed through UV photolysis of H$_2$O$_2$, whereas in the atmosphere, uptake from the gas phase is the dominant known source (Ervens et al., 2003a), with additional contributions from aqueous (e.g., Fenton, nitrate) reactions (Arakaki and Faust, 1998; Zepp et al., 1987). In this work, experimental results are better captured after taking into account the absorption of UV by H$_2$O$_2$ and organic compounds. Finally, the combined glyoxal and methylglyoxal model is used to simulate aqSOA formation via OH radical oxidation under a range of atmospheric conditions, including cloud-relevant conditions (10 µM) and higher concentrations. Runs at 10 M are intended to provide insights into OH radical chemistry in wet aerosols using glyoxal or methylglyoxal as a surrogate for the mix of dissolved water-soluble organics (i.e., based on water-soluble organic carbon compounds of ~ 2–3 µg C m^{-3} and estimated aerosol water concentrations of ~ 10 µg m^{-3} at RH > 70 %; Hennigan et al., 2009; Volkamer et al., 2009). Note that non-radical chemistry is not included in these aerosol SOA yields. Methylglyoxal and glyoxal aqSOA yields are reported for conditions encountered

by clouds and by wet aerosols based on two types of simulations: a "batch reactor" approach, in which the precursor (methylglyoxal or glyoxal) is depleted as OH radical reactions proceed, and a steady-state "continuously stirred tank reactor" (CSTR) approach, in which the precursor is replenished (held constant) in the aqueous phase.

2 Methods

2.1 Experiments used to evaluate chemical modeling

Aqueous methylglyoxal chemistry and yields are developed herein, making use of chemical theory and previously published aqueous photooxidation experiments conducted with OH radicals and methylglyoxal or acetic acid (an intermediate product). Experiments were conducted at cloud-relevant and higher concentrations, but concentrations were still several orders of magnitude lower than the concentrations of water-soluble organic compounds in wet aerosol. Experimental details are provided elsewhere (Tan et al., 2010, 2012). Briefly, methylglyoxal (30, 300, and 3000 µM) or acetic acid (20, 100, and 1000 µM) was dissolved in 18 MΩ Milli-Q water. OH radicals (10^{-14}–10^{-12} M) were generated by photolysis (254 nm with Hg UV lamp) of hydrogen peroxide. Reaction temperature was maintained at ~ 25 °C. Dissolved O$_2$ measured at the beginning and the end of each experiment was saturated. pH decreased from 6.6 to 3.3 over the course of the 360 min experiments. Samples were analyzed by ion chromatography (IC), unit mass resolution electrospray ionization mass spectrometry (ESI-MS), and ESI-MS after preseparation in the IC (IC-ESI-MS). Control experiments were conducted for both organics (methylglyoxal and acetic acid) as follows: organic + UV, organic + H$_2$O$_2$, H$_2$O$_2$ + UV, mixed standard + H$_2$O$_2$, and mixed standard + UV. Mixed standards contained pyruvic, acetic, formic, oxalic, glyoxylic, glycolic, succinic, and malonic acids (250 µM each). Note that H$_2$O$_2$ was measured by the triiodide method (Banerjee et al., 1964) using a UV-visible spectrometer in H$_2$O$_2$ + UV experiments.

2.2 Peroxy radical chemistry

Peroxy radical chemistry plays an important role in the aqueous chemistry of methylglyoxal, which is described in detail in Sect. 3. As in the gas phase, OH radical reactions in the aqueous phase produce peroxy radicals due to the presence of dissolved O$_2$ in atmospheric waters (Herrmann, 2003). Peroxy radicals subsequently undergo two possible reaction pathways: (1) self decomposition giving off HO$_2$ and forming acids, and (2) bimolecular RO$_2$–RO$_2$ reaction. In the glyoxal–OH reaction, glyoxylic acid and oxalic acid are formed by the decomposition pathway, which is also the dominant pathway (Lim et al., 2010). In the methylglyoxal–OH reaction, pyruvic acid is formed by decomposition. However, further OH reactions of pyruvic acid and acetic acid,
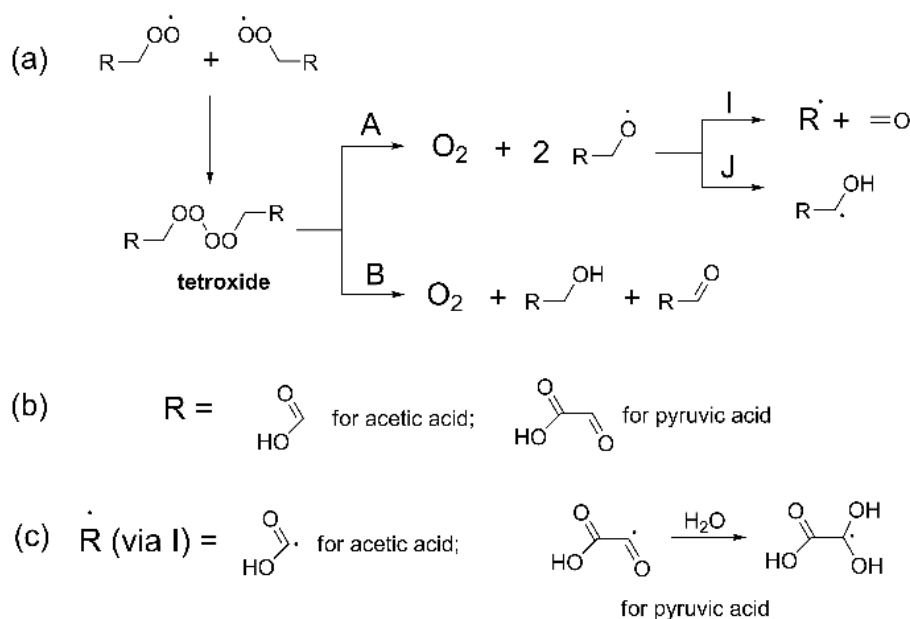
Fig. 1. Mechanism for peroxy radical reactions (**a**). The pathway A is suggested by Benson (1965), forming alkoxy radicals, followed by decomposition (I) or 1,2-hydride shift (J). The pathway B forming no organic radical product (i.e., B is a concerted reaction) is suggested by Russell et al. (1957). Parent precursors can be acetic acid or pyruvic acid (**b**). Fragmented organic radicals (R*) are expected to be stabilized by a carboxylic group for acetic acid ((**c**) left) and a diol, which results from hydration of a carbonyl group for pyruvic acid ((**c**) right).

two major products of the methylglyoxal + OH, involve RO_2–RO_2 reactions.

Figure 1a illustrates peroxy radical chemistry initiated by RO_2–RO_2 reactions. For acetic acid/pyruvic acid + OH reactions, peroxy radicals form by the addition of O_2 to the primary carbon, followed by RO_2–RO_2 reactions forming tetroxides. This pathway is preferred over decomposition because of the absence of a hydroxyl group nearby. Two well-known decomposition pathways from tetroxide are alkoxy radical/O_2 formation (A in Fig. 1a) suggested by Benson (1965), and alcohol/aldehyde/O_2 formation (B in Fig. 1a) suggested by Russell et al. (1957). The Benson pathway (A) and the Russell pathway (B) are not related and are independent because the Russell pathway (B) is a concerted reaction, so none of the products are formed via alkoxy radical chemistry.

Alkoxy radicals formed in the Benson pathway (A) undergo either decomposition (I) or a 1,2-hydride shift (J) (Figs. 1, 2, and 3). In Fig. 1a, resulting products through decomposition of alkoxy radicals (I) are organic radicals (R•) and aldehydes (=O). Gas-phase chamber studies suggest that decomposition of alkoxy radicals is likely to occur if a radical position in an organic radical product (R•) is at secondary or tertiary carbons, and is enhanced when functional groups (e.g, hydroxyl or carboxylic groups) are adjacent to these carbons (Atkinson et al., 2007) due to radical stabilization (Lim and Ziemann, 2009). Alkoxy radicals formed in the aqueous phase contain hydroxyl/carboxylic functional groups since the parent organic precursors are water soluble. Decompo-

sition in the aqueous phase (I) is, therefore, more favorable than in the gas phase. For acetic/pyruvic acid in the aqueous phase (Fig. 1b), alkoxy radicals decompose to organic radicals and formaldehydes. Organic radicals are stabilized by a carboxylic group for acetic acid or a diol (since a carbonyl group will undergo hydration) for pyruvic acid (Fig. 1c), While significant 1,2-hydride shift (followed by O_2 reactions to form carbonyls) is not observed in the gas phase (Atkinson, 2007), alkoxy radicals in the aqueous phase do undergo 1,2-hydride shift. Although the detailed reaction mechanisms are not well understood, the 1,2-hydride shift is very likely to be assisted by water molecules (Von Sonntag et al., 1997).

2.3 Kinetic model

As done previously for glyoxal (Lim et al., 2010), we developed a full kinetic model for aqueous chemistry of methylglyoxal with OH radicals at cloud- and aerosol-relevant concentrations including the following: (1) the formation of organic acids such as acetic, glyoxylic, glycolic, pyruvic, oxalic, and mesoxalic acid (Lim et al., 2005; Tan et al., 2009, 2010, 2012); (2) organic radical–radical reactions to form higher carbon number acids and oligomers; and (3) peroxy radical chemistry, including self decomposition and bimolecular RO_2–RO_2 reactions. The model was first validated by comparison against acetic acid + OH radical experiments (Tan et al., 2012), since acetic acid is an important intermediate product. Then, using the same rate constants, model predictions were compared with concentration dynamics from
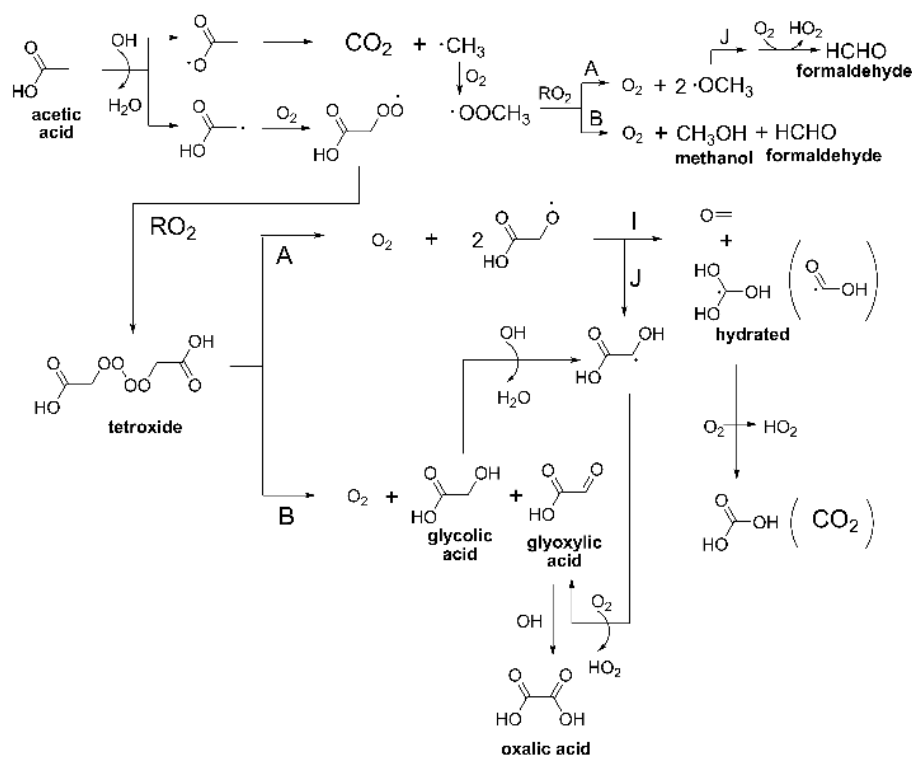
Fig. 2. Reaction mechanisms for the reactions of acetic acid with OH radicals in the aqueous phase. RO_2 represents bimolecular RO_2–RO_2 reactions.

methylglyoxal + OH radical experiments (Tan et al., 2010, 2012).

Most of the kinetic rate constants were obtained from the literature documented in Tan et al. (2009, 2010, 2012), or determined using an estimation method based on structure–activity relationships (Monod et al., 2005, 2008). Values from Ervens et al. (2003b) were also used for OH-radical-initiated reactions. For the radical–O_2 (peroxy radical formation) and organic radical–radical reactions, the rate constants of $1 \times 10^6 \, M^{-1} \, s^{-1}$ and $1.3 \times 10^9 \, M^{-1} \, s^{-1}$, respectively, were used as suggested by Guzman et al. (2006). The following were used for peroxy radical chemistry: a rate constant of $3 \times 10^8 \, M^{-1} \, s^{-1}$ for bimolecular RO_2–RO_2 reactions (Lim et al. 2010), a rate constant of $1 \times 10^7 \, s^{-1}$ for the 1,2-hydride shift (Gilbert et al., 1976), and a rate constant on the order of 10^6 to $10^7 \, s^{-1}$ for decomposition from the alkoxy radical (Gilbert et al., 1981).
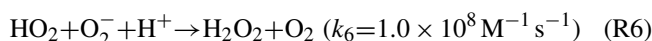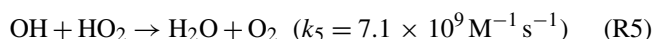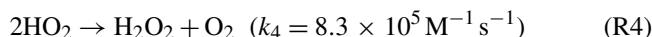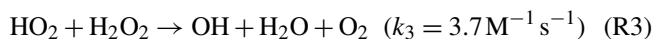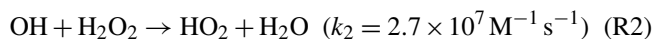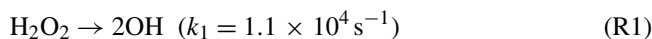
This model, which we describe in detail in Sect. 3, was validated in part by comparison with laboratory experiments and then used to simulate the atmosphere.

2.4 Determining the rate constants for H_2O_2 photolysis

The performance of a glyoxal model (Lim et al., 2010), which includes detailed radical reactions (e.g., H-atom abstraction by OH radicals, peroxy/alkoxy radical reactions, decompositions, and organic radical–radical reactions) was

substantially improved at high concentrations ($\sim$ mM) by including organic radical–radical reactions in the model. Below we describe a further improvement to the glyoxal model that we then apply also to methylglyoxal. Specifically, since OH radicals in *experiments* are produced in situ from H_2O_2 photolysis and H_2O_2 is light absorbing, we correct for light absorption by H_2O_2.

Previously (Tan et al., 2010), the rate constant ($1.1 \times 10^4 \, s^{-1}$) for 254 nm UV photolysis of H_2O_2 at 0.15, 1.5, and 20 mM in experiments was determined by fitting modeled H_2O_2 concentrations (R1–R7) to measurements in H_2O_2 + UV control experiments (Fig. 4a–c) as documented by Tan et al. (2009, 2010, 2012).

$$H_2O_2 \rightarrow 2OH \quad (k_1 = 1.1 \times 10^4 \, s^{-1}) \tag{R1}$$

$$OH + H_2O_2 \rightarrow HO_2 + H_2O \quad (k_2 = 2.7 \times 10^7 \, M^{-1} \, s^{-1}) \tag{R2}$$

$$HO_2 + H_2O_2 \rightarrow OH + H_2O + O_2 \quad (k_3 = 3.7 \, M^{-1} \, s^{-1}) \tag{R3}$$

$$2HO_2 \rightarrow H_2O_2 + O_2 \quad (k_4 = 8.3 \times 10^5 \, M^{-1} \, s^{-1}) \tag{R4}$$

$$OH + HO_2 \rightarrow H_2O + O_2 \quad (k_5 = 7.1 \times 10^9 \, M^{-1} \, s^{-1}) \tag{R5}$$

$$HO_2 + O_2^- + H^+ \rightarrow H_2O_2 + O_2 \quad (k_6 = 1.0 \times 10^8 \, M^{-1} \, s^{-1}) \tag{R6}$$
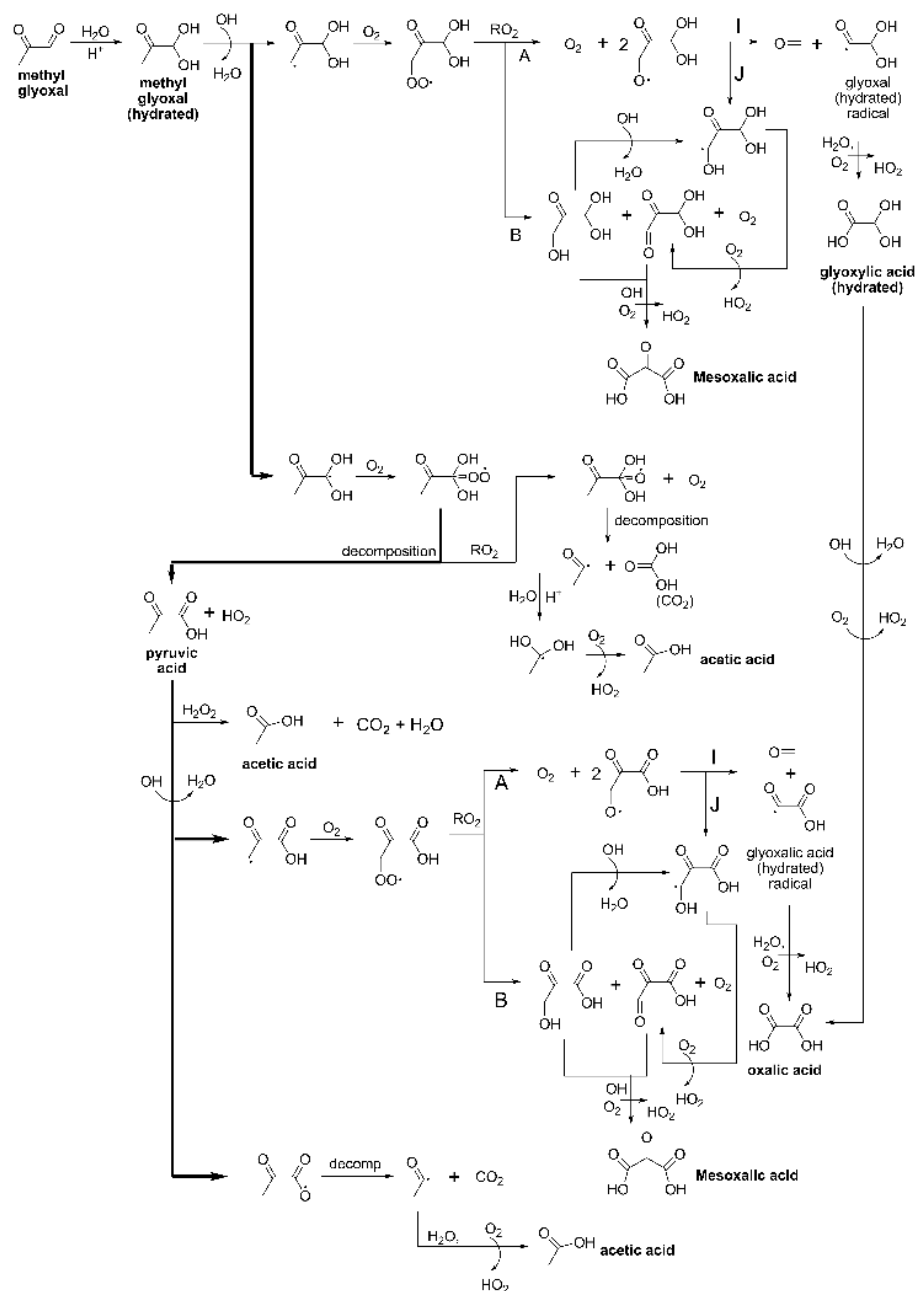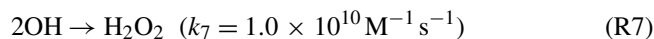
Fig. 3. Reaction mechanisms for the reactions of methylglyoxal with OH radicals in the aqueous phase. The bold arrows represent dominant pathways.

$$2OH \rightarrow H_2O_2 \quad (k_7 = 1.0 \times 10^{10}\,M^{-1}\,s^{-1}) \qquad (R7)$$

However, in the previous work, light absorption by H_2O_2 was not taken into account. The H_2O_2 photolysis rate constant (k_{photo}) can be corrected using Beer's law,

$$k_{\text{photo}}(H_2O_2) = k_1 10^{-b_{\text{ext}} L\,[H_2O_2]} \quad (s^{-1}), \qquad (1)$$

where b_{ext} is extinction coefficient ($M^{-1}\,cm^{-1}$) and L is path length (cm).

An extinction coefficient for H_2O_2 of $18.4\,M^{-1}\,cm^{-1}$ was used (Stefan et al., 1996). A path length of 0.80 cm provides the best fit for all three H_2O_2 concentrations (Fig. 4d–f). This value is reasonable since it is close to the actual path length of the reaction vessel (1.04 cm). Accounting for UV absorption by H_2O_2 provides substantial improvement in the R^2 values at the highest concentration from $R^2 = 0.80$ (Fig. 4a) to 0.96 with correction (Fig. 4d). Thus, in the revised model,

$$k_{\text{photo}}(H_2O_2) = (1.1 \times 10^4)10^{-18.4 \times 0.80 \times [H_2O_2]} \quad (s^{-1}). \qquad (2)$$
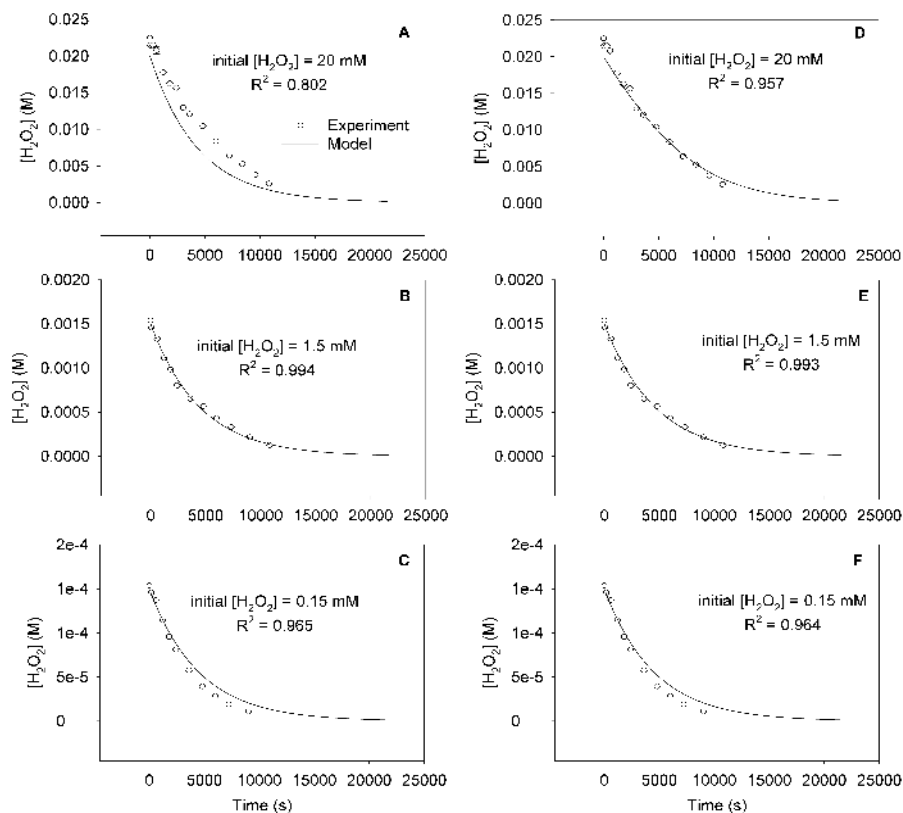
Fig. 4. Real-time profiles of 254 nm UV photolysis decay of H_2O_2 (where initial concentrations are 0.15, 1.5, and 20 mM) without light-absorption correction (**A**, **B**, and **C**) and with the correction (**D**, **E**, and **F**). The correction was made by multiplying the transmittance by the H_2O_2 photolysis decay rate constant, where $-\log$ (transmittance) $= 18.4 \times 0.80 \times [H_2O_2]$.

Methylglyoxal and pyruvic acid are also light-absorbing compounds, and their photolysis reactions are included in the model – methylglyoxal photolysis is even corrected by using extinction coefficient of $12.7 \, M^{-1} \, cm^{-1}$ (Tan et al., 2010). However, these photolysis reactions turn out to be negligible during OH radical reactions because photolysis rates are much slower than OH radical reaction rates (Stefan et al., 1996; Tan et al., 2010).

Both simulated OH concentrations ($\sim 10^{-12}$ M) and simulated and measured pH (3 to 5) reasonably reflect cloud conditions (Faust, 1994; Hermann, 2003). Simulated dissolved O_2 remains saturated during the entire reaction (Fig. S1 in Supplement), in agreement with measured O_2 at the beginning and end of experiments. Note that dissolved O_2 in atmospheric waters is expected to be saturated due to high the surface-to-volume ratio of cloud droplets and wet aerosols.

2.5 Atmospheric simulations

Unlike laboratory experiments, the major source of OH radicals in the *atmospheric* aqueous phase is believed to be uptake from the gas phase, although aqueous sources also contribute (e.g., through Fenton and nitrate reactions; Arakaki

and Faust, 1998; Lim et al., 2005, 2010; Zepp et al., 1987). In atmospheric simulations, the OH radical concentration in the aqueous phase was set to be constant at 2.44×10^{-12} M, a value maintained by Henry's law equilibrium with the gas-phase OH radical concentration of 2×10^6 molecule cm^{-3} (Finlayson-Pitts and Pitts, 2000). This is likely an upper bound, as discussed in Sect. 5. The initial concentration of H_2O_2 in the aqueous phase was set to be zero. The maximum simulated H_2O_2 concentration (largely formed via bimolecular HO_2–HO_2 reactions in the aqueous phase) from photooxidation of 30 μM of initial glyoxal is ~ 20 μM, which is reasonable in atmospheric waters according to Henry's law equilibrium with an atmospheric concentration of H_2O_2 (~ 0.2 ppb) in the gas phase (Warneck, 1999).

The following atmospheric processes are needed to model aqSOA: (1) glyoxal and methylglyoxal production via gas-phase photooxidation, (2) glyoxal and methylglyoxal uptake by atmospheric waters (i.e., Henry's law equilibrium between gas- and aqueous-phase glyoxal and methylglyoxal), (3) uptake or condensed-phase production of oxidants (e.g., OH radicals), (4) aqueous-phase reactions in the atmospheric waters forming low or semivolatile products, and (5) gas–particle partitioning of products. Ideally, all these processes

including detailed aqueous chemistry would be included in the model. When this is not practical, SOA yields can be useful, enabling prediction of SOA by multiplying the amount of "aqueous glyoxal reacted" in a time step by the estimated SOA yield. The production of particle-phase products via aqueous OH radical oxidation (step 4–5) can be approximated in a batch or CSTR framework. In the batch reactor approximation, aqueous-phase OH radical reactions are limited by photochemical production of glyoxal and methylglyoxal in the gas phase. Slow glyoxal/methylglyoxal production results in its depletion in the atmospheric waters by aqueous-phase OH radical reactions. In the CSTR approximation, however, aqueous-phase OH radical reactions are not limited by gas-phase photochemical production of glyoxal and methylglyoxal. In contrast to the batch reactor, glyoxal and methylglyoxal are continuously taken up into atmospheric waters and never depleted in that medium. This is a better assumption when gas-phase production is faster than aqueous reaction. Which of these approximations is more appropriate depends on what the major precursors are in the particular study area. For example, a batch approximation would be appropriate if the dominant methylglyoxal precursors were toluene. The gas-phase lifetime of toluene due to OH (when [OH] in the gas phase is 2×10^6 molecule cm^{-3} (12 h daytime average); Finlayson-Pitts and Pitts, 2000) is ~ 1 day ($k = 5.63 \times 10^{-12}$ cm^3 molecule^{-1} s^{-1}; Atkinson and Arey, 2003) and it produces $\sim 20\%$ methylglyoxal (Nishino et al., 2010). This methylglyoxal can dissolve in cloud/fog waters and react with OH radicals with the lifetime of 4.3 h (when [OH] in the aqueous phase is assumed to be 1×10^{-13} M). A batch approximation is appropriate since in this case the gas-phase production of methylglyoxal is slower than the aqueous-phase OH oxidation of methylglyoxal. In contrast, a CSTR approximation would be more appropriate if the production of methylglyoxal was dominated by compounds like 1,3,5-trimethylbenzene (which produces $\sim 50\%$ methylglyoxal; Nishino et al., 2010). This is because the gas-phase lifetime of 1,3,5-trimethylbenzene due to OH radicals is only 2.5 h. Thus, in this case the gas-phase production of the methylglyoxal precursor is now faster than its aqueous oxidation.

While we expect OH oxidation to be the dominant daytime aqSOA formation pathway in clouds and an important contributor to wet aerosol chemistry (Lim et al., 2010), it should be recognized that the chemistry in wet aerosols is highly complex and poorly understood. Both radical and non-radical reactions are likely to occur in wet aerosols and the relative importance of these pathways may depend on the degree to which OH radicals are produced or recycled in the condensed phase, which is not well understood currently. Undoubtedly, organic–inorganic interactions play an important role in wet aerosol chemistry (e.g., formation of organosulfates and organic nitrogen compounds); the yields reported here are not intended to represent all processes, only aqSOA formed through OH radical reaction.

2.6 SOA yields from atmospheric photochemical simulations

Given

$$A + OH \rightarrow \sum P_i, \tag{R8}$$

where A is glyoxal or methylglyoxal and P_i is product i, the product yield for P_i (Y_{P_i}) is given by

$$Y_{P_i} = \frac{[P_i]}{[A]_{\text{reacted}}}. \tag{3}$$

Then the overall SOA yield (Y_{SOA}) is defined as

$$Y_{\text{SOA}} = \sum F_i Y_i = \frac{\sum F_i [P_i]}{[A]_{\text{reacted}}}, \tag{4}$$

where F_i is the particle fraction of P_i and $[A]_{\text{reacted}}$ is the concentration of unhydrated A reacted with OH radical in the aqueous phase. For glyoxal–OH reactions, the SOA-forming products are oxalate (OXLAC) and oligomers (OLIG). For methylglyoxal–OH reactions, the SOA-forming products are pyruvate (PYRAC), oxalate (OXLAC), and oligomers (OLIG).

To use these yields in a chemical transport model, the model must simulate the gas-phase concentration of A, the uptake of A into the aqueous phase, and the change in the aqueous concentration of A as a result of reactions with OH ($[A]_{\text{reacted}}$) over the course of a time step. $[A]_{\text{reacted}}$ is then multiplied by Y_{SOA} to produce SOA.

2.6.1 Product yield

In the previous glyoxal–OH model, the maximum yields of oxalic acid and oligomers were simulated (Lim et al., 2010), but in this work average yields are estimated. For example, the simulated molar yield of oxalic acid that is formed from the OH-radical-initiated reaction of 10 μM initial [glyoxal] is plotted with the reaction time (x axis) in Fig. 5a. In the previous work (Lim et al., 2010), the maximum yield of 0.91 was estimated. But in this work, Fig. 5a is replotted to 5b, where the x axis is [glyoxal]$_{\text{reacted}}$ and the y axis is [oxalic acid]; therefore, the slope represents the yield of oxalic acid. In Fig. 5b, oxalic acid increases as glyoxal reacts, then the curve drops sharply when glyoxal is depleted. The slope of ~ 0.80, obtained by the linear regression on the product formation curve from the starting point of aqueous-phase photochemistry ($t = 0$) to the peak ($t_{\text{max}} = 38$ min) giving a reasonably low error ($R^2 \sim 0.9$), represents the average (molar) yield of oxalic acid. In CSTR simulation plots, oxalic acid continuously increases and never drops as glyoxal reacts (Fig. 5c). A similar oxalic acid yield (slope = 0.84 with $R^2 \sim 1$) was obtained by linear regression over 60 min of aqueous-phase photochemistry.

Plots of batch simulations conducted from 10 μM to 10 M of initial glyoxal are similar to Fig. 5b ($R^2 \geq 0.9$, $0 \leq t \leq$
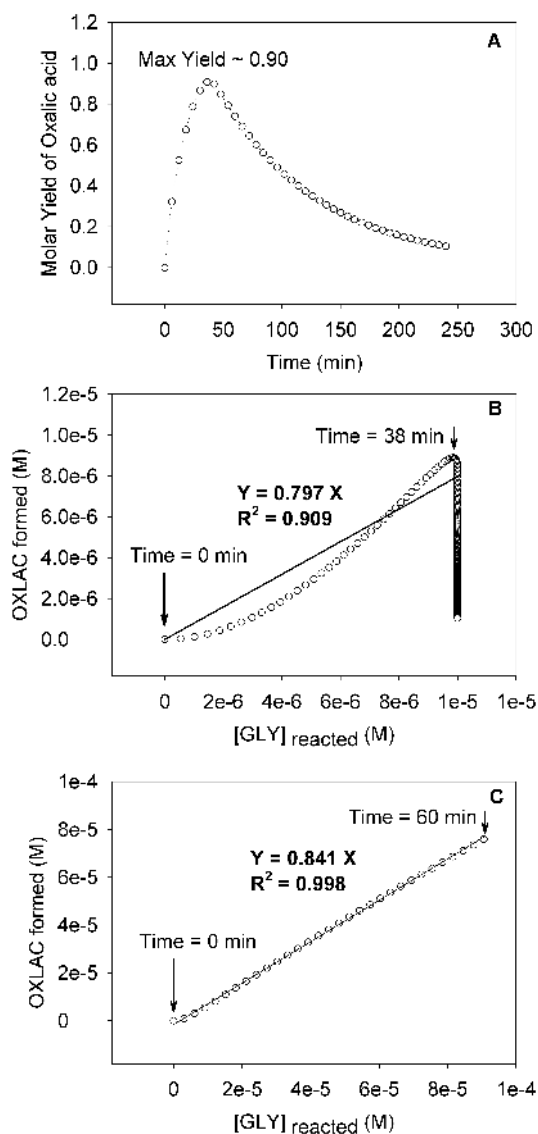
Fig. 5. Simulated results for the OH radical oxidation of glyoxal, where initial [glyoxal] is 10^{-5} M. **(A)** Time profile of oxalic acid yield from the OH radical reactions of glyoxal, batch reactor approximation. The maximum molar yield of ~ 0.9 was estimated previously (Lim et al., 2010). **(B)** Oxalic acid (M) vs. glyoxal reacted (M), batch reactor approximation. In this plot, the linear regression was performed for 0–38 min ($y = 0.797x$, $R^2 = 0.909$), and the slope (0.797) represents the average molar yield of oxalic acid. **(C)** The CSTR simulation, oxalic acid (M) vs. glyoxal reacted (M) for 0–38 min. The average molar yield of oxalic acid (the slope) is 0.841 with higher precision ($R^2 = 0.998$).

t_{max}, 20–40 min), with oxalic acid being the main product below ~ 10 mM and oligomers above ~ 10 mM. Oligomers were calculated as the sum of products with higher carbon number than the precursor (Lim et al., 2010). Plots of CSTR simulations conducted from 0.1 to 100 µM of initial glyoxal

are similar to Fig. 5c ($R^2 \sim 1$, $0 \leq t \leq 60$ min), with oxalic acid being the main product.

2.6.2 Particle fraction

SOA yields also depend on what fraction of each aqueous product remains in the particle phase (Seinfeld and Pankow, 2003). We expect that oligomers stay entirely in the particle phase. In this work, we assume that dicarboxylic acid products of C_3 or higher, such as malonate (C_3) or tartrate (C_4), remain entirely in the particle phase. The gas–particle partitioning of the smaller organic acids (e.g., oxalate, pyruvate) depends on whether they are present in the atmosphere as acids or salts, since their salts have much lower vapor pressures (Limbeck et al., 2001; Martinelango et al., 2007; Smith et al., 2009; Ortiz-Montalvo et al., 2012). For example, the vapor pressure of oxalic acid (at 25 °C) is 8.26×10^{-5} Torr (Saxena and Hildemann, 1996), whereas the vapor pressure of ammonium oxalate is 5.18×10^{-8} Torr (EPA, 2011). In this work, we assume that 90 % of oxalate and 70 % of pyruvate remain in the particle phase (Lim et al., 2005; Ervens et al., 2007). However, these particle fractions could vary based on availability of organic/inorganic constituents (e.g., NH_3, amines, sodium). Note that the yields calculated in this work neglect the formation of glyoxal and methylglyoxal oligomers through droplet evaporation (Loeffler et al., 2006; De Haan et al., 2009).

In summary, SOA yields were estimated using simulation results from glyoxal/methylglyoxal precursor concentrations from 10^{-5} to 10 M, and literature particle fraction values from atmospheric measurements (e.g., 90 % for oxalate, 70 % for pyruvate, and 100 % for oligomers) (Table 1).

3 Aqueous photochemistry of methylglyoxal: mechanisms and kinetic model

3.1 Aqueous-phase reactions of acetic acid with OH radical

Reaction mechanisms for the aqueous-phase OH radical oxidation of acetic acid are proposed in Fig. 2. Acetic acid is oxidized by H-atom abstraction either from OH in the carboxylic group ($*O(O)CCH_3$; $*$ represents radical) or the methyl group ($HO(O)CC*H_2$). [$*O(O)CCH_3$] decomposes to carbon dioxide and a methyl radical ($*CH_3$). This [$*CH_3$] forms [$*OOCH_3$] by O_2 addition and eventually becomes methanol and formaldehyde via RO_2–RO_2 reactions including the Benson/Russell pathways and the alkoxy radical chemistry of decomposition and a 1,2-hydride shift.

The dominant H-atom abstraction from acetic acid occurs from the methyl group with a kinetic rate ~ 5 times faster than abstraction from the carboxylic group (Tan et al., 2012). Through O_2 addition to [$HO(O)CC*H_2$], the peroxy radical [$HO(O)CH_2OO*$] forms, followed by RO_2–RO_2 reactions. In the Benson pathway (A), the alkoxy radical decomposes

Table 1. Product yields, particle-phase product yields and SOA yields.

[Precursor]$_0$ (M)		Y_{OXLAC}		$Y_{OXLAC-P}$		Y_{PYRAC}		$Y_{PYRAC-P}$		Y_{OLIG} (= Y_{OLIG-P})		Y_{SOA}	
[G]$_0$	[MG]$_0$	Batch	CSTR	Batch	CSTR	Batch	CSTR	Batch	CSTR	Batch	CSTR	Batch	CSTR
10^{-7}		1.34	1.32	1.20	1.19					0	0	1.20	1.19
10^{-6}		1.33	1.30	1.20	1.17					0	0	1.20	1.17
10^{-5}		1.34	1.31	1.21	1.17					0	0	1.21	1.17
10^{-4}	N/A	1.28	1.15	1.15	1.03	N/A	N/A	N/A	N/A	0.01	0.01	1.16	1.04
10^{-3}		0.87		0.78						0.08		0.86	
10^{-2}		0.28	N/A	0.25	N/A					0.32	N/A	0.56	N/A
10^{-1}		0.03		0.03						0.68		0.70	
10^0		0		0						0.91		0.91	
10		0		0						0.97		0.97	
	10^{-7}	0.05	0.05	0.05	0.04	1.02	1.09	0.71	0.76	0	0	0.76	0.80
	10^{-6}	0.05	0.05	0.05	0.04	1.02	1.08	0.71	0.76	0	0	0.76	0.80
	10^{-5}	0.12	0.05	0.11	0.04	0.98	1.08	0.68	0.76	0	0	0.79	0.80
N/A	10^{-4}	0.12	0.05	0.11	0.04	0.96	1.03	0.67	0.72	0	0	0.78	0.76
	10^{-3}	0.11		0.10		0.81		0.57		0.03		0.70	
	10^{-2}	0.06	N/A	0.05	N/A	0.56	N/A	0.39	N/A	0.22	N/A	0.66	N/A
	10^{-1}	0.01		0.01		0.13		0.09		0.60		0.70	
	10^0	0		0		0		0		0.90		0.90	
	10	0		0		0		0		0.95		0.95	

[G]$_0$ = initial [glyoxal] (M), [MG]$_0$ = initial [methylglyoxal] (M)
All yields are mass based.
OXLAC = oxalate; PYRAC = pyruvate; OLIG = oligomer
Y_{OXLAC} = OXLAC yield; Y_{PYRAC} = PYRAC yield; Y_{OLIG} = OLIG yield
$Y_{OXLAC-P}$ = particle-phase OXLAC yield; $Y_{PYRAC-P}$ = particle-phase PYRAC yield; Y_{OLIG-P} = particle-phase OLIG yield
$Y_{OXLAC-P} = Y_{OXLAC} \times 0.90$; $Y_{PYRAC-P} = Y_{PYRAC} \times 0.70$; $Y_{OLIG-P} = Y_{OLIG} \times 1$
$Y_{SOA} = Y_{OXLAC-P} + Y_{PYRAC-P} + Y_{OLIG-P}$

to formaldehyde and carbon dioxide, or, via the 1,2-hydride shift, forms [HO(O)CC*H(OH)], which then becomes glyoxylic acid via O_2 reactions and is oxidized further to oxalic acid.

In the Russell pathway (B), the organic products are glycolic acid and glyoxylic acid. OH/O_2 oxidation of glycolic acid forms [HO(O)CH$_2$OO*], which again becomes glyoxylic acid, and is later oxidized to oxalic acid.

Note that Tan et al. (2012) did not observe oligomer formation from the OH radical ($\sim 10^{-12}$ M) oxidation of 1 mM acetic acid, whereas oligomers do form from the OH radical oxidation of glyoxal and methylglyoxal at identical concentrations (Tan et al., 2009, 2010). Oligomers form from glyoxal and methylglyoxal oxidation because of radical stabilization (Guzman et al., 2006; Lim et al., 2010). In the first H-atom-abstracted product of acetic acid (HO(O)C*H$_2$), the radical is rather unstable because it is at the primary carbon. In contrast, for glyoxal/methylglyoxal reactions, the radical is at the triply substituted carbon (i.e., carbon bound to three non-H atoms), and these stabilized radicals allow for oligomers' formation via radical–radical reaction (Lim et al., 2010; Tan et al., 2012). Based on these results, in this kinetic model radical–radical reactions are excluded when the radi-

cal is on the primary carbon (e.g., acetic acid/pyruvic acid–OH radical reactions). Note that organic radical–radical reactions for all organic species except acetic and pyruvic acid are always "turned on" in our model. At low concentrations, organic radical–O_2 reactions are dominant, whereas at high concentrations organic radical–radical reactions are important.

3.2 Aqueous-phase reactions of methylglyoxal with OH radical

Figure 3 illustrates the reaction mechanisms for the aqueous-phase OH radical reaction of methylglyoxal. Major products are pyruvic, acetic, and oxalic acid. Bold arrows indicate the major pathways. Pyruvic acid is the major first-generation product from OH radical reaction of methylglyoxal, and acetic acid is formed substantially from OH radical reactions of pyruvic acid and partially from bimolecular peroxy radical reactions and H_2O_2–pyruvic acid reactions. Oxalic acid is formed directly from glyoxylic and mesoxalic acids, which are products of every pathway shown in Fig. 3.

The first step of the OH radical reactions is H-atom abstraction from the primary carbon (minor) or the carbon in

between the diol (major), then peroxy radical formation by O_2 addition. In the minor pathway, peroxy radicals undergo RO_2–RO_2 reaction, and form alkoxy radicals (the Benson pathway A) or C_3 organic compounds (the Russell pathway B). The alkoxy radical decomposes to formaldehyde and an organic radical compound, and this organic radical later becomes glyoxylic acid. The C_3 organic compounds from the Russell pathway B react with OH radical and eventually form mesoxalic acid. In the major pathway, peroxy radicals either decompose to pyruvic acid while losing HO_2 (major) or undergo RO_2–RO_2 reaction (minor), which eventually leads to the formation of carbon dioxide and acetic acid. It should be noted that pyruvic acid reacts with H_2O_2 and forms acetic acid, carbon dioxide, and water; however this is minor, and OH radical oxidation is the major pathway. The OH radical oxidation of pyruvic acid occurs by H-atom abstraction from the primary carbon or the carboxylic group. The peroxy radical from the radical on the primary carbon forms via O_2 addition, and undergoes RO_2–RO_2 reaction. In this RO_2–RO_2 reaction, oxalic acid and mesoxalic acid are eventually formed via Benson/Russell pathways and alkoxy radical chemistry. The organic radical product from H-atom abstraction from the carboxylic group decomposes to carbon dioxide and a C_2 aldehyde radical, which eventually becomes acetic acid.

3.3 Kinetic model

Reactions and rate/equilibrium constants used in the full kinetic model of glyoxal/methylglyoxal + OH are provided in Table S1. Detailed reaction mechanisms for the decomposition of tetroxides are still not understood, and therefore, calculation of the branching ratio for the two pathways A and B from theory is not possible (Dibble, 2007). In this work, the same branching ratio of 95 % (A) to 5 % (B) was used for acetic and pyruvic acids and methylglyoxal, and this branching ratio was determined based on the ESI-MS intensities of the acetic acid oxidation products and glyoxylic and glycolic acid with an assumption that glycolic acid is only produced in the Russell pathway (B), whereas glyoxylic acid is produced in both the A and B pathways (Figs. 2 and 3). Note that this branching ratio is expected to be independent of initial precursor concentration because decomposition of tetroxides is unimolecular decay.

Although there is a literature rate constant (6×10^7 M^{-1} s^{-1}; Stefan and Bolton, 1999) for the OH radical reaction of pyruvic acid, to our knowledge, there are no detailed literature rate constants for H-atom abstraction from the primary carbon and from the carboxylic group. In this work a branching ratio of 85 % to 15 % (H-atom abstraction from the primary carbon vs. from the carboxylic group) was used based on the estimation method of Monod et al. (2005).

4 Simulation results and discussion

4.1 Model validation: simulating laboratory experiments

Previously, a full kinetic model for the aqueous chemistry of glyoxal with OH radical was developed by including detailed radical chemistry (Lim et al., 2010). In this work, the model was expanded by including comprehensive methylglyoxal–OH radical chemistry: OH radical reactions of acetic acid, pyruvic acid, and methylglyoxal, and light absorption by H_2O_2 and light-absorbing organic compounds (e.g., methylglyoxal, pyruvic acid). The model, then, was validated by simulating the laboratory experiments of Tan et al. (2009, 2010, 2012).

4.1.1 Glyoxal–OH radical model

The light-absorption correction (Sect. 2.4) was validated by simulating glyoxal + OH experiments (Fig. 6). For low-concentration experiments (initial [glyoxal] = 30 μM), oxalic acid predicted by the previous glyoxal model (Lim et al., 2010) and this new model are identical and agree well with the experimental results (Fig. 6a). Simulations are identical because the H_2O_2 concentration (decreasing from 150 μM H_2O_2) was too low to affect photochemistry. H_2O_2 absorbed less than 1 % of the transmitted light, and therefore including light absorption in the model had a negligible effect on OH production from H_2O_2 photolysis. However, the light-absorption correction by H_2O_2 substantially improves the glyoxal–OH radical model simulation (Fig. 6b) at the higher concentration (initial [glyoxal] = 3000 μM), where the initial H_2O_2 concentration was 15 mM (note that higher H_2O_2 concentrations were used in experiments with higher glyoxal/methylglyoxal concentrations in order to maintain similar OH concentrations in all experiments). Note that both the Lim et al. (2010) and the current model include organic radical–radical reactions, resulting in improved prediction of oxalic acid in the 3000 μM experiments compared to the Lim et al. (2005) dilute chemistry model. By correcting for light absorption by H_2O_2 in the current work, the model now captures the timing of the peak (Fig. 6b).

4.1.2 Acetic acid–OH radical model

Next, the performance of the expanded model was evaluated by simulating acetic acid + OH experiments. Model performance was improved by including detailed peroxy radical chemistry: RO_2–RO_2 reactions, the Benson/Russell pathways, and the alkoxy radical chemistry (Fig. 7). In the model, the rate constant for the 1,2-hydride shift from the alkoxy radical is set to be 1×10^7 s^{-1} (Gilbert et al., 1976), while decomposition rates vary: 5×10^6, 8×10^6, and 2×10^7 s^{-1} for initial [acetic acid] = 20, 100, and 1000 μM, respectively. Those values were determined by fitting to the experimental results, while their range is within literature values ($\sim 10^6$–
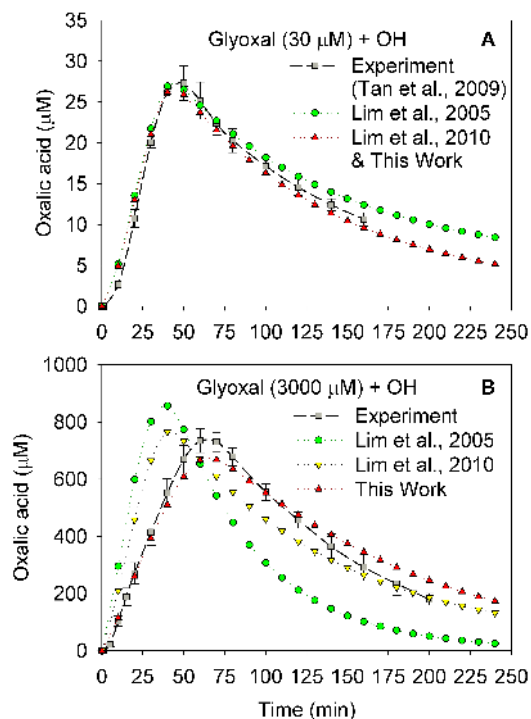
Fig. 6. Real-time profiles of oxalic acid produced from OH radical oxidation of glyoxal at initial concentrations of 30 μM (**A**) and 3000 μM (**B**); experimental results (Tan et al., 2009) and previous/current model simulations (using the model of Lim et al., 2005, 2010; this work).

10^7 s^{-1}) from Gilbert et al. (1981). Ideally, the decomposition rate from the alkoxy radical is constant regardless of the initial acetic acid concentration due to being first order, but pH or cage effects by water molecules could affect the rate.

4.1.3 Methylglyoxal–OH radical model

Simulations of the methylglyoxal + OH experiments are shown in Fig. 8. The methylglyoxal–OH model contains the same parameters used in the acetic acid–OH radical model except the decomposition rate at the initial [methylglyoxal] = 3000 μM is 3.2×10^7 s^{-1} instead of 2×10^7 s^{-1}. Using these values, the performance of the model simulations was substantially improved (Fig. 8a, b). The best fit to the experimental results was obtained by neglecting pyruvic acid photolysis (see comparison, Fig. 8a) rather than including the literature rate constant and product (molar) yields for pyruvic acid photolysis (i.e., pyruvic acid → 0.45 acetic acid + 0.55 CO_2, rate constant = 5×10^{-4} s^{-1}; Carlton et al., 2006). This has been observed previously for similar experiments conducted with acetone (Stefan et al., 1996; Stefan and Bolton, 1999). This is expected because the molar absorptivity of H_2O_2 (Bolton and Carter, 1994) is much larger than the molar absorptivity of pyruvic acid. Thus, photolysis in this experimental system is negligible in the presence of
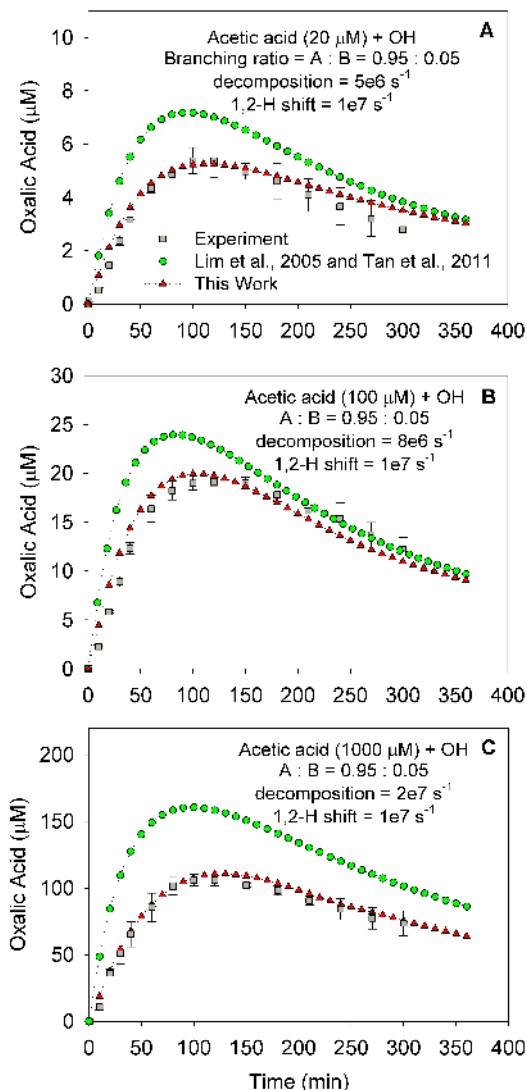

Fig. 7. Real-time profiles of oxalic acid produced from OH radical reactions of acetic acid at the initial acetic acid concentrations of 20 μM (**A**) and 100 μM (**B**) and 1000 μM (**C**); experimental results (Tan et al., 2012) and previous/current model simulations (using the model of Lim et al., 2005; this work).

OH radicals. Note that the purpose of the 254 nm UV lamp in these experiments is to provide an atmospherically relevant OH radical concentration in the aqueous phase and not to study photolysis.

Figure 8c (initial [methylglyoxal] = 3000 μM) is interesting. Although the new model successfully fit oxalate measurements from the OH reactions of 30 and 300 μM of methylglyoxal, at 3000 μM it still does not capture the timing and the magnitude of oxalic acid formation until ∼ 200 min. Accounting for light absorption by H_2O_2 is not sufficient to explain the oxalic acid profile in the 3000 μM methylglyoxal experiments. We hypothesize that this is because of
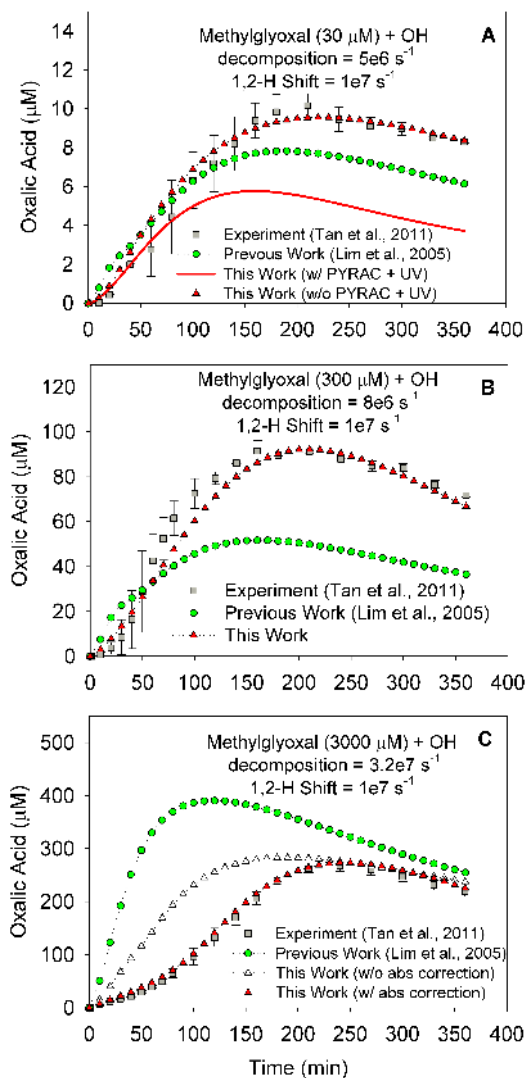
Fig. 8. Real-time profiles of oxalic acid produced from OH radical reactions of methylglyoxal at the initial methylglyoxal concentrations of 30 μM (**A**) and 300 μM (**B**) and 3000 μM (**C**); experimental results (Tan et al., 2012) and previous/current model simulations (using the model of Lim et al., 2005; this work). In (**C**), simulations were performed with and without the absorption (abs) correction by hypothetical light-absorbing organic products, with the same time profile as pyruvic acid, but a much higher extinction coefficient (1500 cm^{-1}M^{-1}).

the formation of light-absorbing organic products that have the same time profile as pyruvic acid but a higher extinction coefficient (1500 cm^{-1} M^{-1}) at 254 nm. Incorporating these "pyruvic acid surrogates" into the model significantly improves the model performance, resulting in an excellent agreement to the experimental values. While we did not identify these light-absorbing products in our reaction vessel, light-absorbing (brown carbon) products of other methylglyoxal reactions have been observed by others. For exam-

ple, Sareen et al. (2010) observed the presence of UV-light-absorbing products with an estimated extinction coefficient of ∼ 5000 cm^{-1} M^{-1} from non-radical reactions of methylglyoxal in highly concentrated aqueous ammonium sulfate solutions. Our methylglyoxal–OH experiments did not contain ammonium sulfate or any other source of nitrogen. In these experiments light absorption could be due to a π-conjugate system formed possibly via aldol condensation (Sareen et al., 2010; Lim et al., 2010; Noziere et al., 2010). Further work is needed to investigate this hypothesis.

4.2 aqSOA yields under atmospheric conditions

According to the field study by Munger et al. (1995), glyoxal and methylglyoxal concentrations in the cloud water are similar, ranging from ∼ 0.1 to 300 μM. For the CSTR runs, 10^{-7}–10^{-4} M glyoxal/methylglyoxal in the aqueous phase were considered. The equivalent gas-phase concentrations due to Henry's law are ∼ 0.3 ppt–0.3 ppb for glyoxal and ∼ 30 ppt–30 ppb for methylglyoxal, and those ranges reasonably agree with literature (Fu et al., 2008). For the batch reactor runs, 10^{-7}–10 M of glyoxal/methylglyoxal concentrations were considered with the highest concentrations comparable to concentrations of water-soluble organics in wet aerosols.

4.2.1 Batch reactor approximation

Mass-based SOA yields for glyoxal and methylglyoxal are obtained using the batch reactor approximation are illustrated in Fig. 9 and summarized in Table 1. At cloud-relevant concentrations, Y_{SOA}Batch(glyoxal) is 1.20 and is solely contributed by oxalate. Y_{SOA}Batch(methylglyoxal) is 0.77, which is the sum of 0.66 from pyruvate and 0.11 from oxalate. Using glyoxal as a surrogate for dissolved water-soluble organics, the aerosol-relevant Y_{SOA}Batch(glyoxal) is 0.94. If instead methylglyoxal is used as a surrogate for total dissolved water-soluble organics, the aerosol-relevant Y_{SOA}Batch(methylglyoxal) is 0.94. Again, this material is predicted to be entirely oligomeric (note that detailed oligomer distributions for 1 M glyoxal and 1 M methylglyoxal are provided in Fig. S3). It should be recognized that the chemistry in wet aerosols is complex and poorly understood. It is unlikely that all dissolved, water-soluble organics in an aerosol particle will have the same ability to form oligomers. However, glyoxal or methylglyoxal are reasonable surrogates for dissolved water-soluble organics because (1) aldehydes and alcohols are the major known water-soluble organic precursors (Blando and Turpin, 2001), (2) they are remarkably reactive to OH radicals in the aqueous phase, (3) and they are expected to have similar oxidation mechanisms.

The total particle-phase yield as a function of concentration is given by

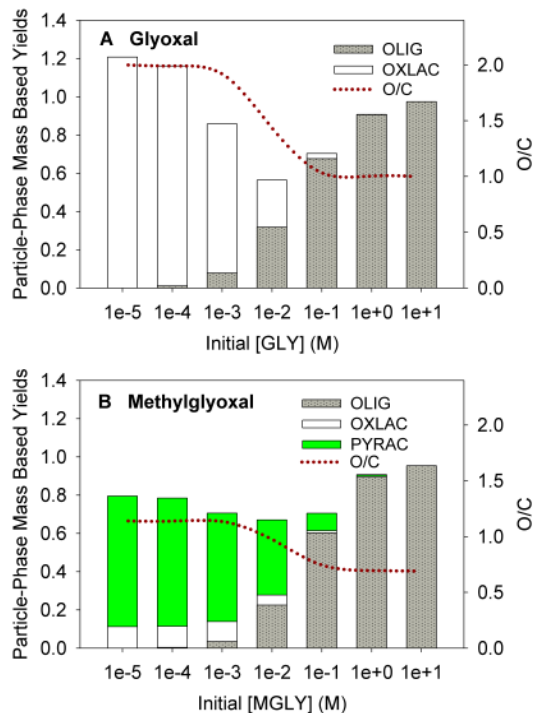$$Y_{SOA}\ (\text{glyoxal}) = \frac{1.20}{1 + 491[G]_0} + \frac{0.931}{1 + \frac{0.0243}{[G]_0}}. \quad (5)$$

Fig. 9. Atmospheric batch simulations **(A)** for particle-phase mass-based yields of oxalate (Y_{OXLAC}), oligomers (Y_{OLIG}), and SOA ($= Y_{OXLAC} + Y_{OLIG}$) with increasing initial concentrations of glyoxal (x axis) for aqueous-phase OH radical reactions, and **(B)** for particle-phase mass-based yields of oxalic acid (Y_{OXLAC}), pyruvate (Y_{PYRAC}), oligomers (Y_{OLIG}), and SOA ($= Y_{OXLAC} + Y_{PYRAC} + Y_{OLIG}$) with increasing initial concentrations of methylglyoxal (x axis) for aqueous-phase OH radical reactions. Similarly, O / C (on the right-hand y axis) vs. initial concentrations of glyoxal **(A)** and O / C vs. initial concentrations of methylglyoxal **(B)**.

Similarly, for methylglyoxal, the total particle-phase yield as a function of concentration is given by

$$Y_{SOA} \text{ (methylglyoxal)} = \frac{0.659}{1 + 71.5[MG]_0}$$
$$+ \frac{0.113}{1 + 107[MG]_0} + \frac{0.940}{1 + \frac{0.0459}{[MG]_0}}, \tag{6}$$

where $[G]_0$ is initial [glyoxal] and $[MG]_0$ is initial [methylglyoxal]. These particle-phase product yields were estimated by fitting to the simulations (Fig. 9a and b) and making use of Eqs. (3) and (4). Note that at 1×10^{-2} M of initial glyoxal in Fig. 9a, the SOA yield is a minimum (56 %) for the following reason. For this initial glyoxal concentration substantial (up to 4.6 mM) H_2O_2 forms by $HO_2 + HO_2$ and $HO_2 + O_2^-$ reactions. The reaction of glyoxylic acid $+ H_2O_2$ forming formic acid competes with the reaction of glyoxylic acid $+$ OH radicals to form oxalate, and also competes with organic radical–radical reactions to form oligomers (Lim et al., 2010). This finding from atmospheric simulation is consistent with previ-

ous experimental results at similar concentrations suggesting a role for H_2O_2 (Lee et al., 2012).

4.2.2 CSTR model

In order to estimate the yield, the reacted glyoxal or methylglyoxal concentrations should be known. Since it is not possible to directly obtain the reacted precursor concentrations in the steady-state CSTR model, they were calculated by summing the major products (e.g., oxalic acid, pyruvic acid, glyoxylic acid, formic acid, acetic acid, formaldehyde, and CO_2), and all of the stoichiometric coefficients are assumed to be 1 except for CO_2, which is 2 because two CO_2 molecules are produced from one oxalic acid molecule. A linear regression method was used to get the product yield during ~ 1 h of glyoxal–OH reaction and ~ 20 min of methylglyoxal–OH reaction (Fig. 5c), resulting in R^2 values close to 1. At cloud-relevant concentrations, Y_{SOA}CSTR(glyoxal) is 1.19 and solely contributed by oxalate (Fig. S2A). Y_{SOA}CSTR(methylglyoxal) is 0.80, which is the sum of 0.76 from pyruvate and 0.044 from oxalate (Fig. S2B). These CSTR yields are quite similar to the batch yields at the same conditions (Fig. 10a and b) and also summarized in Table 1.

4.3 O / C ratio

O / C ratios of aqSOA for glyoxal and methylglyoxal under atmospheric conditions are estimated based on yield fractions of oxalate (O / C $= 2$), pyruvate (O / C $= 1$), and oligomers (Fig. 9a and b). According to FTICR-MS analysis, the O / C ratio of glyoxal oligomers (m/z^- 200–500) is 1.2 (Lim et al., 2010) and the O / C ratio of methylglyoxal oligomers (m/z^- 245–800) is 0.69 (Altieri et al., 2008). O / C ratios decrease from 2 to 1 for glyoxal (Fig. 9a) and from 1 to 0.7 for methylglyoxal (Fig. 9b), as initial concentrations of glyoxal or methylglyoxal increase from cloud conditions to wet aerosol conditions.

5 Conclusions

Volatile but highly water-soluble glyoxal ($\leq 276\,\mu$M – the concentration measured in atmospheric waters), methylglyoxal (0.02–128 μM), and acetic acid/acetate (0.4–245 μM) are common organic compounds found in the atmosphere (Tan et al., 2012). They are mostly gas-phase photochemical fragments of anthropogenic/biogenic VOCs. Due to their small carbon number (C_2-C_3), these compounds form no semivolatile products, and therefore no SOA by gas-phase oxidation alone. However, since they are water soluble, they form SOA via aqueous-phase photochemistry in atmospheric waters. In clouds, the major products of their reaction with OH radicals are oxalate and pyruvate, which remain in the particle phase by forming organic salts with inorganic or ammonium ions. In wet aerosols, the major products are
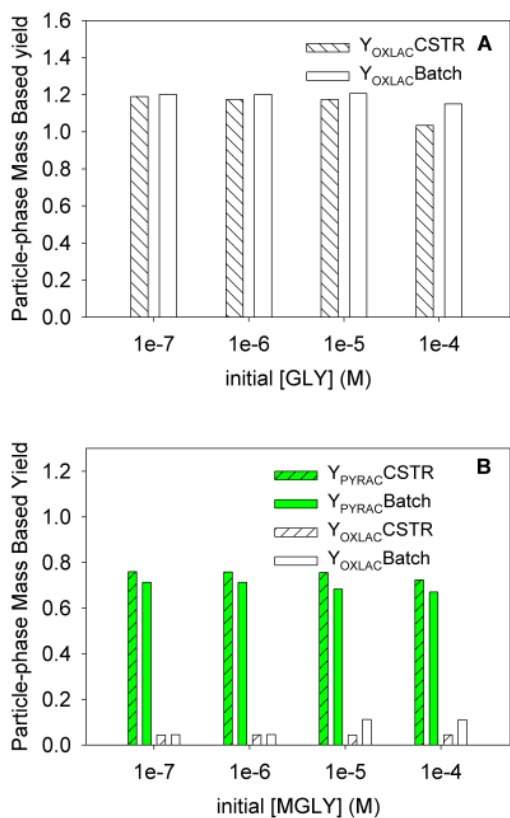
Fig. 10. The CSTR simulation and the batch simulation for particle-phase mass-based yields of oxalate (Y_{OXLAC}) with increasing initial concentrations of glyoxal for glyoxal + OH. **(B)** The CSTR simulation and the batch simulation for particle-phase mass-based yields of pyruvate (Y_{PYRAC}) and oxalate (Y_{OXLAC}) with increasing initial concentrations of methylglyoxal for methylglyoxal + OH.

oligomers, which stay entirely in the particle phase. The aqueous radical chemistry of these compounds is initiated predominantly by OH radicals, and the current understanding is that the main source of aqueous OH radicals is uptake from the gas phase. Peroxy radical chemistry is a key to understanding aqueous-phase OH radical reactions. At cloud-relevant conditions, H-atom-abstracted organic products react with dissolved O_2 forming peroxy radicals, which decompose to carboxylic acids (e.g., glyoxylic acid, oxalic acid, or pyruvic acid) and HO_2. At aerosol-relevant conditions, oligomers are formed via radical–radical reactions. The bimolecular-diffused RO_2–RO_2 reactions constitute important peroxy radical chemistry for OH radical reactions of acetic and pyruvic acid and methylglyoxal. Alcohols and carbonyls are produced in the Russell pathway, whereas alkoxy radicals are produced in the Benson pathway. Alkoxy radicals undergo subsequent decomposition or a 1,2-hydride shift.

In this work, a full kinetic model was developed based on detailed reaction mechanisms and validated against labora-

tory experiments. The batch and CSTR simulations predict similar and substantial aqSOA yields. These simulation results are consistent with the expectation that aqueous chemistry is a substantial source of SOA globally. Although uncertainties are large, recent model studies (Carlton et al., 2008; Fu et al., 2008; Liu et al., 2012) suggest that the magnitude of aqSOA is comparable to SOA formed via gas–particle partitioning of semivolatile products from gas-phase oxidation of VOCs. Certainly, other water-soluble organic precursor will also undergo aqueous chemistry leading to SOA formation.

While glyoxal and methylglyoxal are likely to be present at concentrations up to ∼ 10 mM (in sulfate-containing wet aerosols H_{eff} for glyoxal has been enhanced by a factor of ∼ 500 according to Kampf et al., 2013), our work includes model runs at concentrations as high as molar. In these model runs, glyoxal and methylglyoxal are being treated as surrogates for the complex mixture of water-soluble organics in wet aerosols, recognizing that there are many water-soluble compounds that will exist in atmospheric waters and will form radicals via reaction with OH. In wet aerosols we expect that these radicals will react with each other. Thus, we expect that a complex array of oligomeric products will form in wet aerosols, not just tartaric and malonic acids.

The processes examined in this work depend on the availability of OH radicals in clouds, fogs, and wet aerosols (Waxman et al., 2013). Uptake from the gas phase is generally thought to be the major source of OH radicals to atmospheric waters, and steady-state aqueous concentrations of OH radicals from the gas phase may be influenced by droplet surface-to-volume ratios and aqueous concentrations of reactants. The photo-Fenton reaction (i.e., the photooxidation of Fe ions in the presence of H_2O_2) is considered the major source of OH radicals inside wet aerosols (Arakaki and Faust 1998; Lim et al., 2005, 2010). Photolysis of nitrite/nitrate (Hullar and Anastasio, 2011) and organic matter (Dong and Rosario-Ortiz, 2012) can also produce OH radicals in aqueous particles. However, the degree of OH radical formation or "recycling" in atmospheric waters is not well understood and could represent an important yet unrecognized oxidant source. The sources and fate of oxidants in wet aerosols constitute an important area of current and future research, and may determine to what degree condensed-phase oxidation reactions occur near the surface versus in the bulk of wet aerosols, and the relative importance of radical versus nonradical reactions in aerosols.

Another issue that could impact SOA yields pertains to the gas–particle partitioning of products. The gas–particle partitioning of the carboxylic acid products depends on the extent to which these products are present as carboxylate salts, which have lower vapor pressures than the corresponding acids (e.g., oxalic acid vs. ammonium oxalate; Ortiz-Montalvo et al., 2012). Available measurements put oxalate predominantly in the particle phase, presumably as a salt. However, gas-phase particle partitioning measurements of

carboxylic acids are limited, and this might not be uniformly true.

Supplementary material related to this article is available online at http://www.atmos-chem-phys.net/13/8651/2013/acp-13-8651-2013-supplement.pdf.

References

Altieri, K., Seitzinger, S. P., Carlton, A. G., Turpin, B. J., Klein, G. C., and Marshall, A. G.: Oligomers formed through in-cloud methylglyoxal reactions: chemical composition, properties, and mechanisms investigated by ultra-high resolution FT-ICR Mass Spectrometry, Atmos. Environ., 42, 1476–1490, 2008.

Arakaki, T. and Faust, B. C.: Sources, sinks, and mechanisms of hydroxyl radical (OH) photoproduction and consumption in authentic acidic continental cloud waters from Whiteface Mountain, New York: The role of Fe(r) (r = II, III) photochemical cycle, J. Geophys. Res., 103, 3487–3504, 1998.

Atkinson, R.: Rate constants for the atmospheric reactions of alkoxy radicals: An updated estimated method, Atmos. Environ., 41, 8468–8485, 2007.

Atkinson, R. and Arey, J., Atmospheric degradation of volatile organic compounds, Chem. Rev., 103, 4605–4638, 2003.

Atkinson, R., Baulch, D. L., Cox, R. A., Crowley, J. N., Hampson, R. F., Hynes, R. G., Jenkin, M. E., Rossi, M. J., Troe, J., and IUPAC Subcommittee: Evaluated kinetic and photochemical data for atmospheric chemistry: Volume II – gas phase reactions of organic species, Atmos. Chem. Phys., 6, 3625–4055, doi:10.5194/acp-6-3625-2006, 2006.

Benerjee, D. K. and Budke, C. C.: Spectrophotometric determination of traces of peroxides in organic solvets, Anal. Chem., 36, 792–796, 1964.

Benson, S.: Effects of resonance and structure on the thermochemistry of organic peroxy radicals and the kinetics of combustion reactions, J. Am. Chem. Soc., 87, 972–979, 1965.

Betterton, E. A. and Hoffmann, M. R.: Henry's law constants of some environmentally important aldehydes, Environ. Sci. Technol., 22, 1415–1418, 1988.

Bolton, J. R. and Carter, S. R., Homogeneous photodegradation of pollutants in contaminated water: an introduction, in: Aquatic and Surface Photochemistry, edited by: Helz, G. R., Zeep, R. G., and Crosby, D. G., 467–490, Lewis Publishers, Boca Raton, USA, 1994.

Blando, J. and Turpin, B.: Secondary organic aerosol formation in cloud and fog droplets: a literature evaluation of plausibility, Atmos. Environ., 34, 1623–1632, 2000.

Carlton, A. G., Turpin, B. J., Lim, H. J., Altieri, K. E., and Seitzinger, S.: Link between isoprene and secondary organic aerosol (SOA): Pyruvic acid oxidation yields low volatility organic acids in clouds, Geophys. Res. Lett., 33, L06822, doi:10.1029/2005GL025374, 2006.

De Haan D. O., Corrigan, A. L., Tolbert, M. A., Jimenez, J. L., Wood, S. E., Turley, J. J.: Secondary organic aerosol formation by self-reactions of methylglyoxal and glyoxal in evaporating droplets, Environ. Sci. Technol., 43, 8184–8190, 2009.

Dibble, T. S.: Failures and limitations of quantum chemistry for two key problems in the atmospheric chemistry of peroxy radicals, Atmos. Environ., 42, 5837–5848, 2007.

Dong, M. M. and Rosario-Ortiz, F. L.: Photochemical formation of hydroxyl radical from effluent organic matter, Environ. Sci. Technol., 46, 3788–3794, doi:10.1021/es2043454, 2012.

EPA: Estimation Programs Interface (EPI) Suite™ for Microsoft®Windows, v4.1. Environmental Protection Agency (EPA), Washington, DC, 2011.

Ervens, B., George, C., Williams, J. E., Buxton, G. V., Salmon, G. A., Bydder, M., Wilkinson, F., Dentener, F., Mirabel, P., Wolke, R., and Herrmann, H.: CAPRAM 2.4 (MODAC mechanism): An extended and condensed tropospheric aqueous phase mechanism and its application, J. Geophys. Res., 108, 4426, doi:10.1029/2002JD002202, 2003a.

Ervens, B., Gligorovski, S., and Herrmann, H.: Temperature-dependent rate constants for hydroxyl radical reactions with organic compounds in aqueous solutions, Phys. Chem. Chem. Phys., 5, 1811–1824, 2003b.

Ervens, B., Carlton, A., Turpin, B., Altieri, K. E., Kreidenweis, S. M., and Feingold, G.: Secondary organi aerosol yields from cloud-processing of isoprene oxidation products, Geophys. Res. Lett., 35, L02816, doi:10.1029/2007GL031828, 2007.

Ervens, B., Turpin, B. J., and Weber, R. J.: Secondary organic aerosol formation in cloud droplets and aqueous particles (aqSOA): a review of laboratory, field and model studies, Atmos. Chem. Phys., 11, 11069–11102, doi:10.5194/acp-11-11069-2011, 2011.

Faust, B. C.: Photochemistry of Clouds, Fogs, and Aerosols., Environ. Sci. Technol., 28, 216A–222A, 1994.

Finlayson-Pitts, B. J. and Pitts Jr., J. N.: Chemistry of the upper and lower atmosphere, San Diego, Academic Press, 2000.

Fu, T.-M., Jacob, D. J., Wittrock, F., Burrows, J. P., Vrekoussis, M., and Henze, D. K.: Global budgets of atmospheric glyoxal and methylglyoxal, and implications for formation of secondary organic aerosols, J. Geophys. Res., 113, D15303, doi:10.1029/2007JD009505, 2008.

Gilbert, B. C., Holmes, R. G., Laue, H. A., and Norman, R. O.: Electron spin resonance studies. Part L. Reactions of alkoxy radicals generated from alkyl hydroperoxides and titanium (III) ion in aqueous solution, J. Chem. Soc., Perkin Trans., 2, 1047–1052, 1976.

Gilbert, B. C., Marshall, D. R., Norman, R. O., Pineda, N., and Williams, P. S.: Electron spin resonance studies. Part 61. The generation and reactions of the t-butoxy radical in aqueous solution, J. Chem. Soc., Perkin Trans., 2, 1392–1400, 1981.

Gong, W., Stroud, C., and Zhang, L.: Cloud processing of gases and aerosols in air quality modeling, Atmesphere, 2, 567–616, 2011.

Guzman, M. I., Colussi, A. J., and Hoffmann, M. R.: Photoinduced oligomerization of aqueous pyruvic acid, J. Phys. Chem. A., 110, 3619–3626, 2006.

Hennigan, C. J., Bergin, M. H., Russell, A. G., Nenes, A., and Weber, R. J.: Gas/particle partitioning of water-soluble organic aerosol in Atlanta, Atmos. Chem. Phys., 9, 3613–3628, doi:10.5194/acp-9-3613-2009, 2009.

Herrmann, H.: Kinetics of Aqueous Phase Reactions Relevant for Atmospheric Chemistry, Chem. Rev., 103, 4691–4716, 2003.

Herrmann, H., Tilgner, A., Barzaghi, P., Majdik, Z, Gligorovski, S., Poulain, L., and Monod, A.: Towards a more detailed description of tropospheric aqueous organic chemistry: CAPRAM 3.0, Atmos. Environ., 39, 4351–4363, 2005.

Hullar, T. and Anastasio, C.: Yields of hydrogen peroxide from the reaction of hydroxyl radical with organic compounds in solution and ice, Atmos. Chem. Phys., 11, 7209–7222, doi:10.5194/acp-11-7209-2011, 2011.

Kampf, C. J., Waxman, E. M., Slowik, J. G., Dommen, J., Pfaffenberger, L., Praplan, A. P., Prevot, A. S. H., Baltensperger, U., Hoffmann, T., and Volkamer, R.: Effective Henry's law partitioning and the salting constant of glyoxal in aerosols containing sulfate, Environ. Sci. Technol., 43, 4236–4244, 2013.

Khare, P., Kumar, N., Kumari, K. M., and Srivastava S. S.: Atmospheric formic and acetic acids: An overview, Rev. Geophys., 37, 227–238, 1999.

Lee, A. K., Herckes, P., Leaitch, W. R., Macdonald, A. M., and Abbatt, J. P. D.: Aqueous OH oxidation of ambient organic aerosol and cloud water organics: formation of highly oxidized products, Geophys. Res. Lett., 38, L11805, doi:10.1029/2011GL047439, 2011.

Lee, A. K. Y., Hayden, K. L., Herckes, P., Leaitch, W. R., Liggio, J., Macdonald, A. M., and Abbatt, J. P. D.: Characterization of aerosol and cloud water at a mountain site during WACS 2010: secondary organic aerosol formation through oxidative cloud processing, Atmos. Chem. Phys., 12, 7103–7116, doi:10.5194/acp-12-7103-2012, 2012.

Liao, H. and Seinfeld, J. H.: Global impacts of gas-phase chemistry-aerosol interactions on direct radiative forcing by anthropogenic aerosols and ozone, J. Geophys. Res., 110, D18208, doi:10.1029/2005JD005907, 2005.

Lim, H. J., Carlton, A. G., and Turpin, B. J.: Isoprene forms secondary organic aerosol through cloud processing: model simulations, Environ. Sci. Tech., 39, 4441–4446, 2005.

Lim, Y. B. and Ziemann, P. J.: Kinetics of the heterogeneous conversion of 1,4-hydroxycarbonyls to cyclic hemiacetals and dihydrofurans on organic aerosol particles, Phys. Chem. Chem. Phys., 11, 8029–8039, 2009.

Lim, Y. B., Tan, Y., Perri, M. J., Seitzinger, S. P., and Turpin, B. J.: Aqueous chemistry and its role in secondary organic aerosol (SOA) formation, Atmos. Chem. Phys., 10, 10521–10539, doi:10.5194/acp-10-10521-2010, 2010.

Limbeck, A., Puxbaum, H., Otter, L., and Scholes, M. C.: Semivolatile behavior of dicarboxylic acids and other polar organic species at a rural background site (Nylsvley, RSA), Atmos. Environ., 35, 1853–1862, 2001.

Lin, G., Penner, J. E., Sillman, S., Taraborrelli, D., and Lelieveld, J.: Global modeling of SOA formation from dicarbonyls, epoxides, organic nitrates and peroxides, Atmos. Chem. Phys., 12, 4743–4774, doi:10.5194/acp-12-4743-2012, 2012.

Liu, J., Horowitz, L. W., Fan, S., Carlton, A. G., and Levy II, H.: Global in-cloud production of secondary organic aerosols: Implementation of a detailed chemical mechanism in the GFDL atmospheric model AM3, J. Geophys. Res., 117, D15303, doi:10.1029/2012JD017838, 2012.

Liu, Y., Monod, A., Tritscher, T., Praplan, A. P., DeCarlo, P. F., Temime-Roussel, B., Quivet, E., Marchand, N., Dommen, J., and Baltensperger, U.: Aqueous phase processing of secondary organic aerosol from isoprene photooxidation, Atmos. Chem. Phys., 12, 5879–5895, doi:10.5194/acp-12-5879-2012, 2012.

Loeffler, K. W., Koehler, C. A., Paul, N. M., and DeHann, D. O.: Oligomer formation in evaporating aqueous glyoxal and methyl glyoxal solutions, Environ. Sci. Tech., 40, 6318–6323, 2006.

Martinelango, P. K., Dasgupta, P. K., and Al-Horr, R. S.: Atmospheric production of oxalic acid/oxalate and nitric acid/nitrate in the Tampa Bay airshed: Parallel pathways, Atmos. Environ., 41, 4258–4269, 2007.

McNeill, V. F., Woo, J. L., Kim, D. D., Schwier, A. N., Wannell, N. J., Sumner, A. J., and Barakat, J. M.: Aqueous-phase secondary organic aerosol and organosulfate formation in atmospheric aerosols: a modeling study, Environ. Sci. Technol., 15, 8075–8081, 2012.

Millet, D. B., Donahue, N. M., Pandis, S. N., Polidori, A., Stanier, C. O., Turpin, B. J., and Goldstein, A. H.: Atmospheric volatile organic compound measurements during the Pittsburgh Air Quality Study: Results, interpretation, and quantification of primary and secondary contributions, J. Geophys. Res., 110, D07S07, doi:10.1029/2004JD004601, 2005.

Monod, A. and Doussin, J. F.: Structure-activity relationship for the estimation of OH-oxidation rate constants of aliphatic organic compounds in the aqueous phase: alkanes, alcohols, organic acids and bases, Atmos. Environ., 42, 7611–7622, 2008.

Monod, A., Poulain, L., Grubert, S., Voisin, D., and Wortham, H.: Kinetics of OH-initiated oxidation of oxygenated organic compounds in the aqueous phase: new rate constants, structure-activity relationships and atmospheric implications, Atmos. Environ., 39, 7667–7688, 2005.

Munger, J. W., Jacob, D. J., Caube, B. C., Horowitz, L. W., Keene, W. C., and Heikes, B. G.: Formaldehyde, glyoxal, and methylglyoxal in air and cloudwater at a rural mountain site in central Virginia, J. Geophys. Res., 100, 9325–9333, 1995.

Myriokefalitakis, S., Tsigaridis, K., Mihalopoulos, N., Sciare, J., Nenes, A., Kawamura, K., Segers, A., and Kanakidou, M.: In-cloud oxalate formation in the global troposphere: a 3-D modeling study, Atmos. Chem. Phys., 11, 5761–5782, doi:10.5194/acp-11-5761-2011, 2011.

Nishino, N., Arey, J., and Atkinson, R.: Formation yields of glyoxal and methylglyoxal from the gas-phase OH radical-initiated reactions of toluene, xylenes, and trimethylbenzenes as a function of NO$_2$ concentration, J. Phys. Chem. A, 114, 10140–10147, 2010.

Nolte, C. G., Fraser, M. P., and Cass, G. R.: Gas phase C2-C10 organic acids concentrations in the Los Angeles atmosphere, Environ. Sci. Technol., 33, 540–545, 1999.

Noziere, B., Dziedzic, P., and Cordova, A.: Inorganic ammonium salts and carbonate salts are efficient catalysts for aldol condensation in atmospheric aerosols, Phys. Chem. Chem. Phys., 12, 3684–3872, 2010.

Ortiz-Montalvo, D. L., Lim, Y. B., Perri, M. J., Seitzinger, S. P., and Turpin, B. J.: Volatility and yield of Glycolaldehyde SOA formed through aqueous photochemistry and droplet evaporation, Aerosol Sci. Technol., 46, 1002–1014, 2012.

Russell, G. A.: Deuterium-isotope effects in the autoxidation of aralkyl hydrocarbons. mechanism of the interaction of peroxy radicals, J. Am. Chem. Soc., 79, 3871–3877, 1957.

Sareen, N., Schwier, A. N., Shapiro, E. L., Mitroo, D., and McNeill, V. F.: Secondary organic material formed by methylglyoxal in aqueous aerosol mimics, Atmos. Chem. Phys., 10, 997–1016, doi:10.5194/acp-10-997-2010, 2010.

Saxena, P. and Hildemann, L. M.: Water-soluble organics in atmospheric particles: a critical review of the literature and application of thermodynamics to identify candidate compounds, J. Atmos. Chem., 24, 57–109, 1996.

Seinfeld, J. H. and Pankow, J. F.: Organic atmospheric particulate material, Ann. Rev. Phys. Chem., 54, 121–140, 2003.

Smith, J. N., Barsanti, K. C., Friedli, H. R., Ehn, N., Kulmala, M., Collins, D. R., Scheckman, J. H., Williams, B. J., and McMurry, P. H.: Observation of aminium salts in atmospheric nanoparticles and possible climatic implications, P. Natl. Acad. Sci., 107, 6634–6639, doi:10.1073/pnas.0912127107, 2009

Stefan, M. I. and Bolton, J. R.: Reinvestigation of the acetone degradation mechanism in dilute aqueous solution by the UV/H$_2$O$_2$ process, Environ. Sci. Technol., 33, 870–873, 1999.

Stefan, M. I., Hoy, A. R., and Bolton, J. R.: Kinetics and mechanism of the degradation and mineralization of acetone in dilute aqueous solution sensitized by the UV photolysis of hydrogen peroxide, Environ. Sci. Technol., 30, 2382–2390, 1996.

Tadic, J., Moortgat, G. K., and Wirtz, K.: Photolysis of glyoxal in air, J. Photochem. Photobiol. A: Chem., 177, 116–124, 2006.

Tan, Y., Perri, M. J., Seitzinger S. P., and Turpin, B. J.: Effects of precursor concentration and acidic sulfate in aqueous glyoxal-OH radical oxidation and implications for secondary organic aerosol, Environ. Sci. Technol., 43, 8105–8112, 2009.

Tan, Y., Carlton, A. G., Seitzinger, S. P., and Turpin, B. J.: SOA from methylglyoxal in clouds and wet aerosols: measurements and prediction of key products, Atmos. Environ., 44, 5218–5226, 2010.

Tan, Y., Lim, Y. B., Altieri, K. E., Seitzinger, S. P., and Turpin, B. J.: Mechanisms leading to oligomers and SOA through aqueous photooxidation: insights from OH radical oxidation of acetic acid and methylglyoxal, Atmos. Chem. Phys., 12, 801–813, doi:10.5194/acp-12-801-2012, 2012.

Volkamer, R., Ziemann, P. J., and Molina, M. J.: Secondary Organic Aerosol Formation from Acetylene (C$_2$H$_2$): seed effect on SOA yields due to organic photochemistry in the aerosol aqueous phase, Atmos. Chem. Phys., 9, 1907–1928, doi:10.5194/acp-9-1907-2009, 2009.

Von Sonntag, C., Dowideit, P., Fang, X., Mertens, R., Pan, X., Schuchmann, M. N., and Schuchmann, H.: The fate of peroxyl radicals in aqueous solution, Wat. Sci. Tech., 53, 9–15, 1997.

Warneck, P.: The relative importance of various pathways for the oxidation of sulfur dioxide and nitrogen dioxide in sunlit continental fair weather clouds, Phys. Chem. Chem. Phys., 1, 5471–5483, 1999.

Waxman, E. M., Dzepina, K., Ervens, B., Lee-Taylor, J., Aumont, B., Jimenez, J. L., Madronich, S., and Volkamer, R.: Secondary organic aerosol formation from semi- and intermediate-volatility organic compounds and glyoxal: Relevance of O/C as a tracer for aqueous multiphase chemistry, Geophys. Res. Lett., 40, 978–982, doi:10.1002/grl.50203, 2013.

Zepp, R. G., Holgne, J., and Bader, H.: Nitrate-induced photooxidation of trace organic chemical in water, Environ. Sci. Technol., 21, 443–450, 1987.

Zhou, Y., Zhang, H., Parikh, H. M., Chen, E. H., Rattanavaraha, W., Rosen, E. P., Wang, W., and Kamens, R. M.: Secondary organic aerosol formation from xylenes and mixtures of toluene and xylenes in an atmospheric urban hydrocarbon mixture: Water and particle seed effects (II), Atmos. Environ., 45, 3882–3890, 2011.